

## 17.2 PARAMETERIZED MESOSCALE FORCING MECHANISMS FOR INITIATING NUMERICALLY-SIMULATED ISOLATED MULTICELLULAR CONVECTION

Adrian M. Loftus \*, Charles A. Doswell III, Daniel B. Weber, and Benjamin C. Baranowski  
University of Oklahoma, Norman, Oklahoma

### 1. INTRODUCTION

The interaction among various atmospheric scales with regard to initiating and sustaining deep moist convection is an intriguing and complex issue. Environments generally favorable for long-lived deep moist convection typically are provided in midlatitudes by synoptic-scale systems, and some mechanism, such as surface heating or ascent along surface boundaries, is usually required to lift moist air from near the surface to its Level of Free Convection (LFC) and thereby initiate deep moist convection. The ascent associated with these mechanisms plays an important role in the development and maintenance of many convective events (Doswell 1987). Some numerical simulations of deep moist convection (hereafter, DMC) have shown that variation in the structure and evolution of this ascent can lead to significant differences in the resulting convection (Crook and Moncrieff 1988; McPherson and Droegemeier 1991; Xin and Reuter 1996).

Of interest to the current numerical study is the relationship between the initiation and maintenance of *non-precipitating* DMC and the characteristics of the mesoscale forcing involved in producing the convection. This topic was investigated in two-dimensional numerical simulations of DMC carried out by Crook and Moncrieff (1988) (hereafter, CM88). CM88 reported that cold pool forcing was not always necessary to sustain DMC - other factors such as mesoscale forcing can play a role in the redevelopment of convective cells. The present work builds off the results of CM88 and examines differences in the convective response to various convective initiation mechanisms as the first step in a project to understand updraft regeneration frequency in isolated multicellular deep convection. The goal is the implementation of a parameterized mesoscale lifting mechanism that can initiate and sustain deep convection in a numerical cloud model.

An overview of convective initiation (hereafter, CI) methods in numerical cloud models is provided in section 2. Section 3 outlines the numerical model and parameters used in this study, along with the methodology to parameterize mesoscale ascent in the cloud model. Section 4 details the simulations performed using three CI methods with idealized environmental conditions. The conclusions attained from this study and some proposed future applications using the constant flux methods are given in section 5.

### 2. BACKGROUND

Cloud model simulations have been used extensively to understand the key processes that govern the developments and lifecycles of various types of convection. An initial buoyant perturbation (referred to here as an "initiating bubble" or "IB") has been used traditionally in numerical cloud models to generate the ascent needed to initiate DMC (e.g., Schlesinger 1975; Klemp and Wilhelmson 1978; Weisman and Klemp 1982, among others). Though this approach is simple and provides useful results, it is unphysical and additional forcing is often needed for long-lasting DMC to develop. Another issue with IBs is that the ensuing convection is sensitive to the IB characteristics (Weisman and Klemp 1982, 1984; McPherson and Droegemeier 1991). A more physically realistic method to initiate sustained convection within the framework of a numerical cloud model is through the continuous application of controlled mesoscale ascent (Hill 1977; Tripoli and Cotton 1980; Schlesinger 1982; CM88; Carpenter et al. 1998).

The constant heat flux is one approach used to provide steady forced mesoscale ascent and is based on the idea that insolation-produced diabatic heating within the Planetary Boundary Layer (PBL) leads to thermals capable of initiating DMC. Simulations by Hill (1974, 1977), and Balaji and Clark (1988) successfully demonstrated both the initiation of DMC and the regeneration of convective updrafts when a constant heat flux was applied. Carpenter et al. (1998) applied a non-uniform, constant surface heat flux to generate cumulus congestus clouds and observed periodic oscillations in maximum vertical velocity and cloud water content. The focus of this latter study was not DMC, though the pulsating nature of the clouds in response to continuous forcing is representative of sustained multicellular convection.

An alternative method to generate continuous mesoscale ascent is through steady momentum flux forcing. This mechanism has typically been implemented in numerical cloud models via horizontal convergence-divergence coupling (Chang and Orville 1973; Chen and Orville 1980; Xin and Reuter 1996), or by an assumed vertical velocity profile and associated adjustment of the horizontal wind fields (Tripoli and Cotton 1980). Results from these investigations illustrate that the inclusion of mesoscale ascent typically enhances the strength and duration of convective activity. Also evident in these studies is that persistent ascent acts to destabilize the initial environment and thereby hasten the development of deep convection.

CM88 developed a method for initiating and sustaining multicellular convection in their 2-D numerical

---

\* *Corresponding author address:* Adrian M. Loftus, Colorado State Univ., Dept. of Atmos. Sci., Fort Collins, CO, 80523-1371; email: aloftus@atmos.colostate.edu

cloud model via assimilation of the perturbation fields associated with an imposed constant-amplitude, mesoscale internal gravity wave. The authors conducted experiments with and without precipitation and concluded that the dependence of the convective system on the development of a cold pool to maintain the system was not of vital importance in the presence of large-scale convergence, although cold pool forcing did act to strengthen the convection overall.

Forced mesoscale ascent pre-conditions the atmosphere for DMC in the simulations by weakening any existing low-level temperature inversions (Chen and Orville 1980) and deepening the moist layer (see also Beebe 1958). In our study, the natural mesoscale processes capable of initiating DMC are parameterized using constant momentum and heat flux approaches. Although not physically realistic, these approaches serve to represent processes that would otherwise require grid-nesting procedures to incorporate. The essential idea behind a constant flux is that mesoscale ascent persists much longer than the convective time scale (hours versus minutes), so the initiating lift is effectively steady in comparison with the resulting deep convection. Therefore, these flux methods mimic the real process by which convection is initiated, but do not incorporate all the complexities of those real processes.

### 3. MODEL DESCRIPTION AND METHODOLOGY

The three-dimensional non-hydrostatic numerical cloud model ARPI3D (see Weber 1997 for details), developed at the Center for Analysis and Prediction of Storms (CAPS), is used in the present study to perform the simulations of deep moist convection in the presence of mesoscale forcing. This fully compressible model is based largely on the Advanced Regional Prediction System (ARPS) model developed by CAPS at the University of Oklahoma (see Xue et al. 2000). The initialization of the horizontally homogeneous base state variables in ARPI3D follows that of the ARPS model, and moisture components are governed by the Kessler (1969) warm rain microphysics.

The model domain size used in the present study is 48 x 48 x 20 km in the  $x$ ,  $y$ , and  $z$ , directions, respectively, and the grid spacing is 400 m and 200 m in the horizontal and vertical directions, respectively. The model is run out to 150 minutes to allow the convective responses to the initiating mechanism to be observed and the DMC to evolve through several convective cycles. The large and small time step sizes for the model simulations are 5 and 0.5 seconds, respectively, unless otherwise specified.

#### 3.1 IB and constant heat flux techniques

An initial potential temperature perturbation  $\theta'$  is prescribed by

$$\theta' = \theta'_{\max} \cos^2 \left[ \sqrt{\left(\frac{x-x_c}{x_{rad}}\right)^2 + \left(\frac{y-y_c}{y_{rad}}\right)^2 + \left(\frac{z-z_c}{z_{rad}}\right)^2} \right] \quad (3.1)$$

where  $x_c$ ,  $y_c$ , and  $z_c$ , define the centroid of the bubble,  $x_{rad}$ ,  $y_{rad}$ , and  $z_{rad}$  are the radii of the bubble in the  $x$ ,  $y$ , and  $z$  directions, respectively, and  $\theta'_{\max}$  is the maximum magnitude of the perturbation. The model  $\theta'$  field is initialized using Eq. (3.1) for both the IB and constant heat flux methods, but unlike the IB method in which the buoyant bubble is prescribed only at the beginning of the simulation, the constant heat flux approach continuously reinforces the bubble perturbation throughout the simulation. This serves to provide a source region of constant buoyancy to initiate deep convection, analogous to that observed over an island on a sunny day.

#### 3.2 Low-level convergence field

The parameterized low-level ascent method assumes there is no divergence associated with the background flow in this layer; that is, any divergence is related solely to the imposed mesoscale perturbations added to the background flow. The incompressible mass continuity equation is used to relate the assumed mesoscale vertical velocity gradient to the horizontal divergence of the mesoscale perturbation horizontal velocity, where  $u'_m$  and  $v'_m$  are the magnitudes of the zonal and meridional mesoscale perturbation velocities, respectively, and  $w'$  is the magnitude of the forced (mesoscale) vertical velocity.

Implementation of this in the model involves imposing velocity perturbations within the forcing layer, so specifying the divergence field requires a way to determine those velocity perturbations. This is done through the development of a perturbation velocity potential that has a Gaussian shape in the horizontal and decreases in magnitude with height (Eq 3.2).

$$\phi_m(x, y, z) = Af(z) \exp\left[-\left(\frac{x-x_c}{\lambda_x}\right)^2\right] \exp\left[-\left(\frac{y-y_c}{\lambda_y}\right)^2\right] \quad (3.2)$$

$x_c$  and  $y_c$  are the horizontal coordinates of the center of the ascent region,  $\lambda_x$  and  $\lambda_y$  are 'shape control parameters' of the divergence field in the  $x$  and  $y$  directions, respectively,  $A$  is a constant that determines the maximum forcing magnitude, and  $f(z)$  is a linear function defined as

$$f(z) = 1 - \frac{z_{sfc} - z}{z_{sfc} - z_{deep}}, \quad (3.3)$$

where  $z_{sfc}$  is the physical surface height and  $z_{deep}$  is the depth of the forcing region. The shape control parameters are used to prescribe the horizontal width and ellipticity of the forcing region. The horizontal components of the perturbation flow are given in terms of the velocity potential and divergence is simply the horizontal Laplacian of  $\phi_m$ . From (3.2) and (3.3), it is seen that the maximum magnitude for the divergence ( $D_{max}$ ) occurs at  $(x_c, y_c, z_{sfc})$ .

To prevent the forced flow pattern from interacting with the lateral boundaries and to ensure that no change in net mass occurs within the system, a lower bound is

set on the minimum horizontal domain size of the model, such that the perturbation flow goes to zero within the boundaries. Thus, the maximum values of  $\lambda_x$  and  $\lambda_y$  depend on the horizontal domain size.

Inclusion of the mesoscale perturbation velocities  $u'_m$  and  $v'_m$  causes the model dynamics to be unbalanced at the start, and the model adjusts rapidly to this imbalance by creating a region of ascent within and directly above the forcing zone. For points above the forcing layer, values of  $u'_m$  and  $v'_m$  are initially set to zero and evolve according to the model's governing equations. Base state horizontal wind components ( $\bar{u}$  and  $\bar{v}$ ) are added to the computed values of  $u'_m$  and  $v'_m$  to produce the full  $u$  and  $v$ , thereby superimposing the specified convergence field flow onto the background flow. The horizontal velocities contained within the specified forcing layer are overwritten at the end of each small time step. This process causes the magnitudes of the forced mesoscale horizontal wind components therein to remain fixed throughout the simulation, resulting in a continuously forced convergent flow field within the specified volume, as intended.

#### 4. EXPERIMENTAL SIMULATIONS

Simulations were conducted to determine the effects of the constant heat and momentum flux methods on the development of DMC. The background environment (Fig. 1) is taken to be horizontally homogeneous. The PBL is approximately 800 m deep and is not well mixed with respect to moisture. A stable layer exists between the PBL top and roughly 1400 m to suppress the weaker convection and allow only the stronger convective cells to develop, as often occurs in the real atmosphere. The LFC for a surface parcel is at a height of 710 m, just below the stable layer, resulting in a maximum calculated value of Convective Available Potential Energy (CAPE) of approximately  $2900 \text{ J kg}^{-1}$ . Since the boundary layer mixing ratio varies, the LFC height (and the resulting CAPE value) changes according to the ascending parcel source level. Thus, parcels originating above the surface level have a different LFC height than those originating at the surface. Weak unidirectional shear is present in the 850 to 300 hPa layer and is intentionally less than shear typically associated with supercells.

Model solutions for each experiment are diagnosed by examining the distribution of cloud water mixing ratios ( $q_c$ ) and time series depictions of the domain-wide the maximum vertical velocities ( $w_{max}$ ) associated with the strongest convective updrafts.

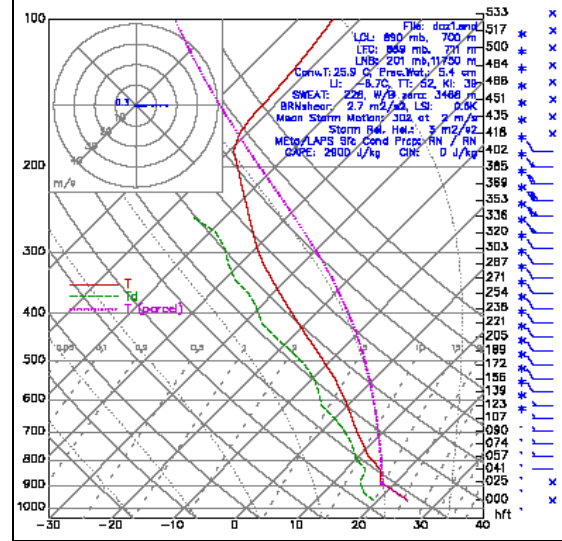


Figure 1: Skew-T plot of background environmental vertical profiles of temperature, moisture, and winds used in all simulations

#### 4.1 Initiating bubble (IB) experiments

A set of simulations (Table 1) utilizing the 'IB' approach is performed primarily for comparison purposes with the simulations using the constant forcing methods. The horizontal radii of the IBs are 5 km, the vertical extent varies between 600 and 1400 m, and the value of  $\theta'_{max}$  is 1 K. The IBs are centered in the horizontal domain, at  $x = y = 24 \text{ km}$ . The height of the IB center above the surface equals the vertical radius for full ellipsoidal bubbles, whereas the IB center is located at the surface for half-ellipsoidal bubbles.

For the sake of brevity, only the key results obtained from these IB simulations are presented. As expected, DMC is not sustained beyond the initial convective development in all cases (Fig. 2) due to the lack of additional forcing. Also, as the vertical extent of the IB increases, the time required for CI to occur increases in the full IB cases (Fig. 2a), whereas the timing of CI for the half bubbles is observed to be largely independent of vertical extent (Fig. 2b). Lastly, the values of  $w_{max}$  attained by the convection are nearly equal at  $25 \text{ m s}^{-1}$  and  $22.5 \text{ m s}^{-1}$  for the full and half bubble cases, respectively. These latter results agree with those from McPherson and Droegemeier (1991) and Brooks (1992) which suggest that, for equal magnitude perturbations, the initial convective intensity may be much more sensitive to the IB width rather than its vertical extent.

Full Ellipsoid	$z_{rad}$ (m)	$z_c$ (m)	Half Ellipsoid	$z_{rad}$ (m)	$z_c$ (m)
IBFUL1, HEATFUL1	300	300	IBHLF1, HEATHLF1	600	0
IBFUL2, HEATFUL2	400	400	IBHLF2, HEATHLF2	800	0
IBFUL3, HEATFUL3	500	500	IBHLF3, HEATHLF3	1000	0
IBFUL4, HEATFUL4	600	600	IBHLF4, HEATHLF4	1200	0
IBFUL5, HEATFUL5	700	700	IBHLF5, HEATHLF5	1400	0

Table 1: Names and parameter values for the IB and constant heat flux (HEAT) experiments.

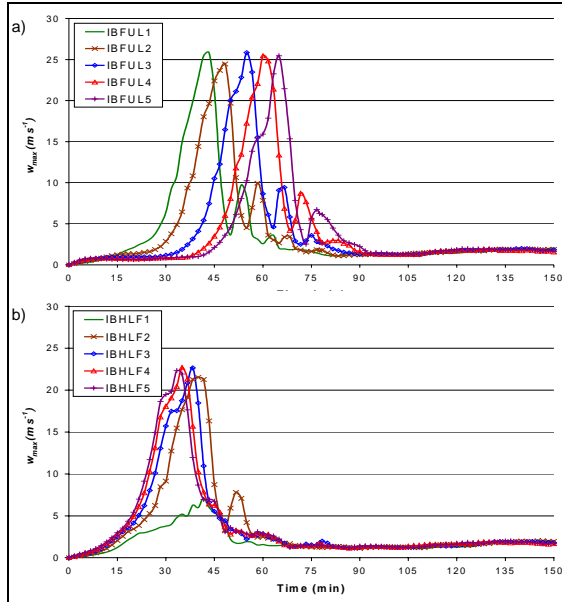


Figure 2: Time series of domain-wide  $w_{max}$  ( $m s^{-1}$ ) values for IB experiments for a) full ellipsoid bubbles and b) half ellipsoid bubbles.

#### 4.2 Constant heat flux experiments

Parameters identical to those utilized in the IB experiments are used to define the perturbations in the constant heat source simulations (Table 1). The simulations are performed using stable large and small time steps of 2.5 and 0.25 seconds, respectively. The sensitivity of the solution to the depth and height of the heated source region is investigated via an examination of the domain-wide  $w_{max}$  values over time.

Inspection of  $w_{max}$  values for the full ellipsoid regions (Fig. 3a) shows DMC is initiated in all 5 cases. Initial peak updraft speeds of approximately  $25 m s^{-1}$  are observed for regions with vertical radii of 300 to 500 m, and increases in initial peak  $w_{max}$  values are evident as  $Z_{rad}$  of the source region increases above 500 m. This result suggests that convective intensity is correlated with the total amount of heat input for source regions that extend beyond 1000 m in the vertical, though no such relationship is evident for smaller source regions.

Initiation of DMC in the 'half ellipsoid' experiments (Fig. 3b) only occurs for cases HEATHLF3, HEATHLF4, and HEATHLF5. The source regions in these three cases have vertical radii of 1000 m or greater, and initial peak updraft speeds appear to increase as  $Z_{rad}$  increases, similar to results observed in the full ellipsoid cases. On the other hand, DMC does not develop for forcing regions with the smallest vertical diameters, HEATHLF1 and HEATHLF2, in which peak  $w_{max}$  values of only about  $3 m s^{-1}$  are observed.

As the vertical extent of the heat source increases, the time required for the initial DMC to develop decreases. Unlike the results for the IB cases, this result seems to be independent of the vertical location of  $\theta'_{max}$ . These results generally suggest that the sooner buoyant parcels erode the stable layer from below, the sooner CI occurs.

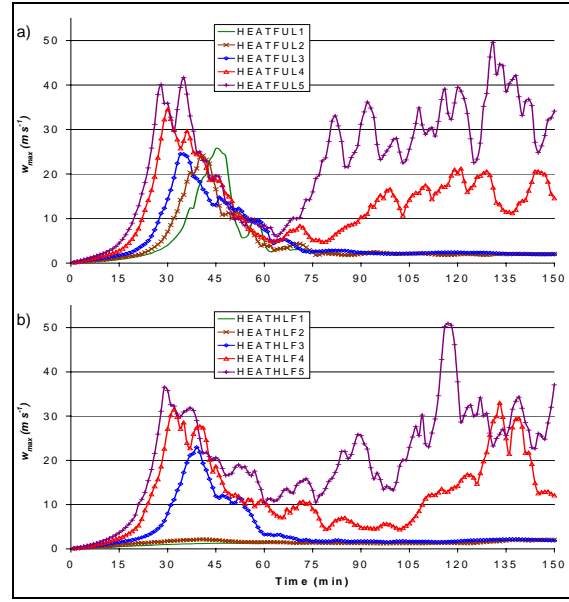


Figure 3: Time series of domain-wide  $w_{max}$  ( $ms^{-1}$ ) values for constant heat flux experiments for a) full ellipsoid source regions and b) half ellipsoid source regions.

Substantial increases in  $w_{max}$  (Fig. 3), corresponding to regeneration of DMC, are observed after approximately 75 minutes for both full and half ellipsoid heating regions with a vertical extent of 1400 m (HEATFUL5 and HEATHLF5). New convective development is also evident in cases HEATFUL4 and HEATHLF4 beyond 90 minutes; however, interactions between the initial convection and the lateral boundaries may be influencing the model solution by this time. No additional convection is generated for the other heat source simulations suggesting that the vertical extent of the forcing region may be a determining factor as to whether or not redevelopment of DMC occurs.

#### 4.3 Momentum flux experiments

Table 2 summarizes the various combinations of the convergence field parameters investigated in this set of experiments. The indicated ranges for the forcing parameters are by no means definitive. Rather, they have been chosen to determine general trends in the convective responses as the characteristics of the forcing are altered.

As the forcing magnitude is increased (Fig. 4a), the time required for DMC to become established decreases. This result agrees qualitatively with Xin and Reuter (1996) who found that an earlier onset of surface rainfall (and thus an earlier onset of convection) was correlated with an increase in the magnitude of low-level convergence. Also evident is the average increase in updraft speed as the forcing magnitude increases. Thus, the intensity of the convection appears to be directly related to the magnitude of  $D_{max}$  for simulations in which the volume of the forcing region remains constant. This is consistent with results found by Tripoli and Cotton (1980) that related rainfall intensity, and hence

Run Name	$D_{max}$ ( $s^{-1}$ )	$z_{deep}$ (m)	$\lambda_x, \lambda_y$ (m)
CONTROL	$-1.0 \times 10^{-3}$	1000	5000
CONVMAG1	$-1.0 \times 10^{-4}$	1000	5000
CONVMAG2	$-5.0 \times 10^{-4}$	1000	5000
CONVMAG3	$-7.5 \times 10^{-4}$	1000	5000
CONVMAG4	$-2.5 \times 10^{-3}$	1000	5000
CONVMAG5	$-5.0 \times 10^{-3}$	1000	5000
CONVDEEP1	$-1.0 \times 10^{-3}$	600	5000
CONVDEEP2	$-1.0 \times 10^{-3}$	800	5000
CONVDEEP3	$-1.0 \times 10^{-3}$	1200	5000
CONVDEEP4	$-1.0 \times 10^{-3}$	1400	5000
CONVWIDE1	$-1.0 \times 10^{-3}$	1000	2500
CONVWIDE2	$-1.0 \times 10^{-3}$	1000	7500
CONVWIDE3	$-1.0 \times 10^{-3}$	1000	10000

Table 2: Names and range of parameters tested for the forced convergence field experiments.

convective intensity, directly to the strength of the low-level convergence in simulations of DMC over Florida.

For the current set of sensitivity tests, once DMC has been initiated, recurrent convective cells develop in all of the simulations except for CONVMAG1 (Fig. 4a). Apparently, in agreement with common meteorological reasoning, if the ascent in the forcing region is too weak, DMC will not be initiated. Also observed is an apparent decrease in the convective updraft regeneration period as the forcing magnitude increases, where the regeneration period is defined as the elapsed time between two subsequent peaks in  $w_{max}$ . For example, as the forcing magnitude increases from  $|-5.0 \times 10^{-4} s^{-1}|$  to  $|-5.0 \times 10^{-3} s^{-1}|$ , the regeneration period decreases from approximately 20 minutes to 10 minutes.

CI is observed to occur at similar times for cases in which the forcing layer depths range from 1000 to 1400 m (Fig. 4b). As the forcing layer depth is decreased below 1000 m, CI is delayed until later in the simulation, similar to findings by Xin and Reuter (1996). In the current study, the deeper forcing layers in cases CONVDEEP3, CONVDEEP4, and CONVDEEP5 extend above the PBL top, such that air parcels in the stable layer are incorporated into the forced ascent region by the convergent flow. Incorporation of this stably stratified air with the less stably-stratified air in the PBL essentially decreases the local stability of the stable layer more rapidly than would occur by turbulent mixing from below the stable layer alone.

A definitive pattern between forcing layer depth and convective intensity ( $w_{max}$ ) is not evident for the range of depths investigated. This is in contrast to findings by Xin and Reuter (1996) in which convective intensity was observed to increase as the convergence layer depth increased. In their study, however, they used a 2D model and a sounding that was more conditionally unstable than that used in the current work, as well as allowed for evaporative cooling effects, so a direct comparison between studies may not be possible.

Further examination of Fig. 4b shows that increasing the depth of the forcing layer appears to cause a decrease in the period of updraft regeneration. Redevelopment of DMC is absent in the CONVDEEP1 simulation, suggesting that either much of the energy provided by the forcing is exhausted after the initial convective development, or the atmospheric stability is modified locally to prevent additional development.

Development of DMC is observed for all cases in Fig. 4c, except the smallest horizontal forcing area case (CONVWIDE1) for which peak magnitudes of  $w_{max}$  attain values of only  $5 m s^{-1}$  by 90 minutes. These results suggest that the horizontal width of the convergence region is an important factor in determining whether or not CI occurs for the specified forcing magnitude and layer depth. A general increase in updraft intensity with increasing forcing region width observed in Fig. 4c is consistent with CM 88, who reported that the amount of lifting of environmental air was directly proportional to the width of their forcing region. More specifically, they demonstrated that the air within the forcing region experienced a larger total vertical displacement for wider convergence zones than for smaller forcing regions, causing parcels to undergo longer periods of forced ascent and eventually leading to more vigorous convective updrafts. The vertical displacement of air

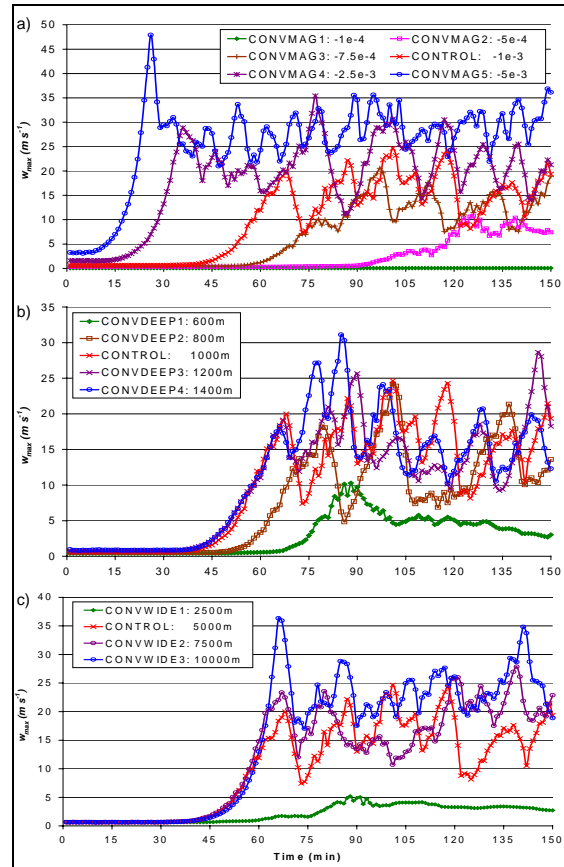


Figure 4: Time series of  $w_{max}$  for momentum flux forcing simulations. Variations in (a) forcing magnitude  $D_{max}$  (magnitudes  $[s^{-1}]$  listed in legend), (b) forcing layer depth ( $z_{deep}$  values listed in legend), and (c) forcing region width ( $\lambda_x$  and  $\lambda_y$  values listed in legend).

parcels within and just above the convergence zone in the CONVWIDE1 case is apparently insufficient for CI.

For the three simulations in which DMC is initiated in Fig. 4c, the time required for CI to occur does not appear to be affected by the width of the convergence region. We have already shown that timing of CI is strongly related to the magnitude of the forced ascent provided by the convergent flow. The maximum magnitude of the forced ascent is largely independent of  $\lambda_x$  and  $\lambda_y$ , so even though the horizontal area over which air is forced to rise varies, the maximum magnitude of this forced ascent is equal in all cases. It seems logical, therefore, that CI occurs at similar times.

Figure 4c also shows that convective updrafts continue to redevelop throughout the remainder of the simulations beyond the initial CI. Though not as evident as in the previous two sensitivity tests, a wider forcing area appears to cause a decrease in the average regeneration period of the convective updrafts.

#### 4.4 Comparison between different CI methods

The initial perturbations in these comparisons consist of similar spatial dimensions of  $10 \times 10 \times 1.2$  km in the horizontal and vertical directions, respectively. The maximum potential temperature perturbation ( $\theta'_{max}$ ) for the IB and constant heat flux cases is located at the surface, as is the maximum convergence magnitude in the momentum flux case. The perturbations vanish at a height of 1.2 km in each case. Vertical cross sections of the  $q_c$  fields depict the early (Fig. 5, frames a, b, and c) and later (Fig. 5, frames d, e, and f) stages of convective development for the three cases. Different times are needed in the momentum flux initiation case because the initial convection produced via a convergent flow field takes longer to develop.

There are obvious differences in the structure of the convective clouds produced by the different initiation mechanisms, especially in the later phases of development. The elapsed simulation time between the early and later phases of convection for each case is 21 minutes, however, the evolution and structure of the convection in each simulation is remarkably dissimilar within this timeframe. In the IB case (Fig. 5d), the DMC is in its dissipating stage and only the upper portion of the original cloud remains, as expected. The constant heat flux simulation (Fig. 5e) shows DMC in its mature stage, consisting of several updrafts in close proximity to one another such that they appear merged into a single updraft. The distribution of  $q_c$  in the momentum flux simulation (Fig. 5f) is associated with three separate convective entities, suggesting that DMC is occurring in several discrete stages.

In general, DMC generated in the constant heat flux case (HEATHLF4) attains the greatest peak magnitude of  $w_{max}$  ( $\sim 30 \text{ m s}^{-1}$ ) among these three simulations (Fig. 6), and the peak  $w_{max}$  value is slightly larger in the momentum flux case (CONVDEEP4) than in the IB case (IBHLF4). The results for this particular set of simulations certainly show that the intensity of the DMC is sensitive to the CI mechanism. The IBHLF4 case only exhibits one convective cycle between

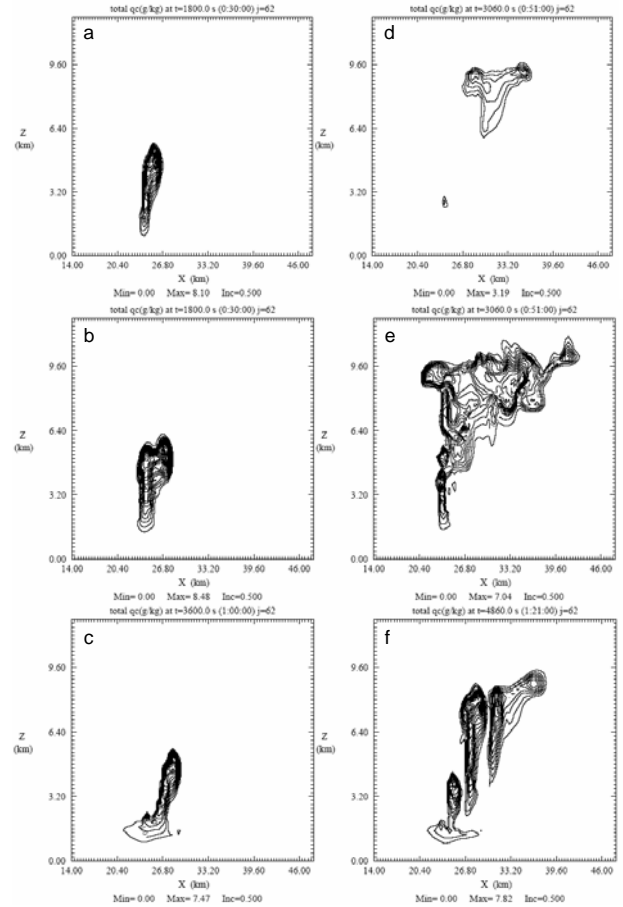


Figure 5: Cloud water content ( $\text{g kg}^{-1}$ ) for an IB case (top row), a constant heat source case (middle row) and a forced convergence case (bottom row). Simulation times for the top two rows of plots are at  $t = 30$  and 51 minutes for left and right columns, respectively, and plots in the bottom row are at  $t = 60$  and 81 minutes for left and right columns, respectively. Contour intervals are  $0.5 \text{ g kg}^{-1}$ , and tick marks are 400 m in the horizontal and 200 m in the vertical.

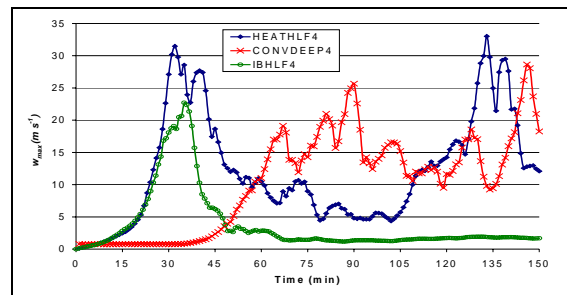


Figure 6: Time series of  $w_{max}$  ( $\text{m s}^{-1}$ ) for three different CI methods.

approximately 15 and 50 minutes simulation time, as does the HEATHLF4 case. However, the period of the cycle in this constant heating simulation appears to last longer than in the IB case, as shown by the slower rate of decrease in the  $w_{max}$  magnitudes between 35 and 65 minutes. Several separate peaks in  $w_{max}$  are displayed in CONVDEEP4 between 60 and 90 minutes, corresponding to the multiple updrafts in Fig. 5f.

## 5. PRELIMINARY CONCLUSIONS

Simulations of non-precipitating DMC have been performed to compare three different initiation mechanisms using the three-dimensional numerical cloud model ARPI3D. The key findings of this study are summarized as follows.

All of the IB simulations demonstrated a lack of redevelopment of convection without precipitation-induced cold pools. The constant heat flux method generated sustained DMC that was, on average, more intense than what was observed in the similar IB cases. Updraft intensity was found to be proportional to the vertical extent of the heat source region and CI took longer to occur as the depth of the heating region was decreased. Redevelopment of convection was observed when the heat source region extended several hundred meters into the stable layer.

The momentum flux method implemented in this study appears adequate to represent mesoscale forcing to initiate DMC in a physically realistic fashion in a numerical cloud model. The time required for CI was found to depend primarily on the maximum divergence value and the forcing layer depth. Increases in the magnitudes of the maximum divergence and horizontal size of the convergence field also led to intensity increases in all of the cases examined. Regeneration of convective updrafts was observed in nearly all cases in which CI occurred, and the period of regeneration tended to decrease as the magnitudes of each of the forcing parameters increased.

The three different initiation methods revealed clear differences in the development and structure of the ensuing deep moist convection, especially during the later stages of development. Differences in convective intensity among the three CI mechanisms were observed as well, though it is difficult to quantify the cause of this as the physical characteristics of the forcing associated with each method are different.

The simulations performed in this study appear to demonstrate the ability of the continuous forcing techniques to initiate and maintain non-precipitating DMC, but in order to gain a more complete understanding of how the forcing interacts with the environment and the forcing-induced convection, further tests are planned. Sensitivity tests will be done to make certain that the pertinent characteristics of the solutions are not resolution-dependent. Droegemeier et al. (1994) reported sensitivity of the maximum updraft speeds to resolution in simulations of supercells, and Bryan et al. (2003) demonstrated differences in the convective overturning of updrafts as grid resolution is increased in simulations of linear convection.

Differences in environmental factors with respect to the resulting convection type have not been considered in the present study. These aspects will be addressed in a non-dimensional parameter range study as part of a larger investigation of isolated multicellular convection. This study will examine a system of combined parameters that describe the convective atmosphere in terms of the initiating mechanism as well as the ambient profiles of temperature, moisture, and winds.

*Acknowledgements.* The authors wish to thank Alan Shapiro, Evgeni Federovich, and Lance Leslie of the University of Oklahoma (OU) for their valuable input, Fred Carr of OU for TA funding during the course of this project, and Henry Neeman and the staff at the Oklahoma Supercomputing Center for Research and Education (OSCR). This research was funded in part by National Science Foundation Grant #ATM-0350539.

## REFERENCES

- ARPS, 1995: ARPS Users Guide Version 4.0, Center for Analysis and Prediction of Storms, Univ. of Okla., 380pp.
- Balaji, V. and T. L. Clark, 1988: Scale selection in locally forced convective fields and the initiation of deep cumulus. *J. Atmos. Sci.*, **45**, 3188-3211.
- Beebe, R.G., 1958: Tornado proximity soundings. *Bull. Amer. Meteor. Soc.*, **39**, 195-201.
- Brooks, H. E., 1992: Operational implications of the sensitivity of modeled thunderstorms to thermal perturbations. *Preprints, Fourth AES/CMOS Workshop on Operational Meteorology*, Whistler, BC, Canada, Atmospheric Environment Service and Canadian Meteorological and Oceanographic Society, 398-407.
- Bryan, G. H., J. C. Wyngaard, and J. M. Fritsch, 2003: Resolution requirements for the simulation of deep moist convection. *Mon. Wea. Rev.*, **131**, 2394-2416.
- Carpenter, R. L., Jr., K. K. Droegemeier, and A. M. Blyth, 1998: Entrainment and detrainment in numerically simulated cumulus congestus clouds. Part I: General results. *J. Atmos. Sci.*, **55**, 3417-3432.
- Chang, S. W. and H. D. Orville, 1973: Large-scale convergence in a numerical cloud model. *J. Atmos. Sci.*, **30**, 947-950.
- Chen, C. and H. D. Orville, 1980: Effects of mesoscale convergence on cloud convection. *J. Appl. Meteor.*, **19**, 256-274.
- Crook, N. A. and M. W. Moncrieff, 1988: The effect of large-scale convergence on the generation and maintenance of deep moist convection. *J. Atmos. Sci.*, **45**, 3606-3624.
- Doswell, C. A., III, 1987: The distinction between large-scale and mesoscale contribution to severe convection: A case study example. *Wea. Forecasting*, **2**, 3-16.
- Droegemeier, K. K., G. Bassett, and M. Xue, 1994: Very high resolution, uniform-grid simulations of deep convection on a massively parallel computer: Implications for small-scale predictability. *Preprints, 10<sup>th</sup> Conference on Numerical Weather Prediction*, Portland, OR, American Meteorological Society, 376-379.
- Hill, G. E., 1974: Factors controlling the size and spacing of cumulus clouds as revealed by numerical experiments. *J. Atmos. Sci.*, **31**, 646-673.
- \_\_\_\_\_, 1977: Initiation mechanisms and development of cumulus convection. *J. Atmos. Sci.*, **34**, 1934-1941.
- Kessler, E., 1969: *On the Distribution and Continuity of Water Substance in Atmospheric Circulation. Meteorological Monographs*, No. 32, American Meteorological Society, 84 pp.
- Klemp, J. B., and R. B. Wilhelmson, 1978: The simulation of three-dimensional convective storm dynamics. *J. Atmos. Sci.*, **35**, 1070-1096.
- McPherson R. A. and K. K. Droegemeier, 1991: Numerical predictability experiments of the May 20 1977 Del City, OK supercell storm. *Preprints, 9<sup>th</sup> Conference on Numerical Weather Prediction*, Denver, CO, American Meteorological Society, 734-738.
- Schlesinger, R. E., 1975: A three-dimensional numerical model of an isolated deep convective cloud: Preliminary results. *J. Atmos. Sci.*, **32**, 934-957.
- \_\_\_\_\_, 1982: Effects of mesoscale lifting, precipitation and boundary-layer shear on severe storm dynamics in a three-dimensional numerical modeling study. *Preprints, 12<sup>th</sup> Conference on Severe Local Storms*, San Antonio, TX, American Meteorological Society, 536-541.
- Tripoli, G. J. and W. R. Cotton, 1980: A numerical investigation of several factors contributing to the observed variable intensity of deep convection over South Florida. *J. Appl. Meteor.*, **19**, 1037-1063.
- Weber, D. B., 1997: An investigation of the diurnal variability of the central Colorado downslope windstorm. Ph.D. Dissertation, The University of Oklahoma, 242pp. [Available from School of Meteorology, University of Oklahoma, 100 E. Boyd, Norman, OK 73019].
- Weisman, M. L. and J.B. Klemp, 1982: The dependence of numerically simulated convective storms on vertical wind shear and buoyancy. *Mon. Wea. Rev.*, **110**, 504-520.
- \_\_\_\_\_, and \_\_\_\_\_, 1984: The structure and classification of numerically simulated convective storms in directionally varying wind shears. *Mon. Wea. Rev.*, **112**, 2479-2498.
- Xin, L. and G.W. Reuter, 1996: Numerical simulation of the effects of mesoscale convergence on convective rain showers. *Mon. Wea. Rev.*, **124**, 2828-2842.
- Xue, M., K. K. Droegemeier, and V. Wong, 2000: The Advanced Regional Prediction System (ARPS) - A multiscale nonhydrostatic atmospheric simulation and prediction tool. Part I: Model dynamics and verification. *Meteorology and Atmospheric Physics*, **75**, 161-193.